Tension-Induced Error Correction and Not Kinetochore Attachment Status Activates the SAC in an Aurora-B/C-Dependent Manner in Oocytes

Antoine Vallot, Ioanna Leontiou, Damien Cladière, Warif El Yakoubi, Susanne Bolte, Eulalie Buffin, Katja Wassmann

Graphical Abstract

Click here to download Graphical Abstract graphical abstract R2 bis.ai

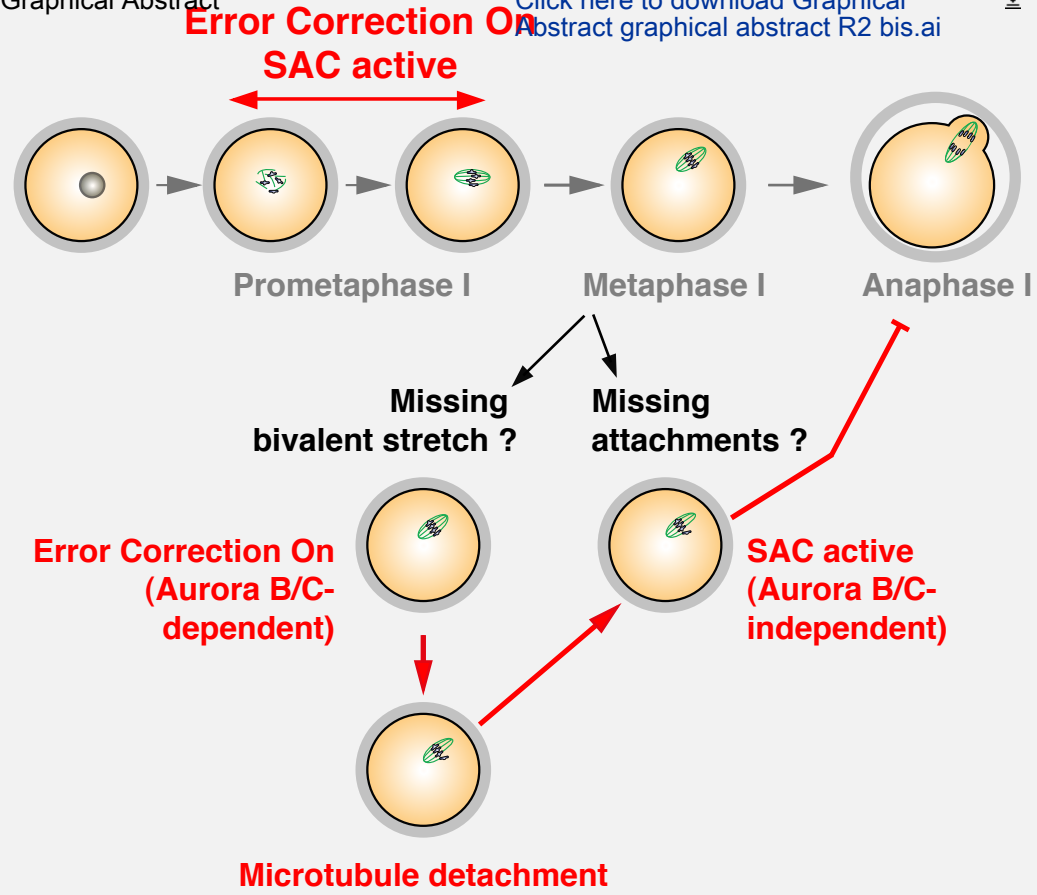

Tension-induced error correction and not kinetochore attachment status activates the SAC in an Aurora B/C-dependent manner in oocytes

Antoine Vallot[1, 2], Ioanna Leontiou[1, 2, 3], Damien Cladière[1, 2], Warif El Yakoubi[1, 2], Susanne Bolte[1, 4], Eulalie Buffin[1, 2, 6], and Katja Wassmann[1, 2, 5, 6]

[1]Sorbonne Universités, UPMC Univ Paris 06, CNRS FRE3631 Institut de Biologie Paris Seine (IBPS), 7 Quai St. Bernard, Paris, 75005 France

[2]CNRS UMR7622 Developmental Biology Lab, 7 Quai St. Bernard , 75005, Paris, France

[3]present address: Wellcome Trust Centre for Cell Biology, University of Edinburgh, Max Born Crescent, Edinburgh, EH9 3JR, UK

[4]CNRS FRE3631, IBPS Imaging Facility, 7 Quai St. Bernard, 75005, Paris, France

[5]Lead contact

[6]Corresponding authors: Eulalie Buffin (eulalie.buffin@upmc.fr) and Katja Wassmann (katja.wassmann@upmc.fr)

Tel.: +33 1 44 27 33 01

Fax: +33 1 44 27 34 45

Keywords: Meiosis, Error Correction, Spindle Assembly Checkpoint, Aurora B/C kinase, Bivalent stretch, Microtubule Attachment, Mouse oocytes

Running Title: Error correction upon loss of bivalent stretch in mouse oocytes

Summary

Cell division with partitioning of the genetic material should take place only when paired chromosomes named bivalents (meiosis I), or sister chromatids (mitosis, meiosis II) are correctly attached to the bipolar spindle in a tension-generating manner. For this to happen, the spindle assembly checkpoint (SAC) checks whether unattached kinetochores are present, in which case anaphase onset is delayed to permit further establishment of attachments. Additionally, microtubules are stabilized when they are attached and under tension. In mitosis, attachments not under tension activate the so-named error correction pathway depending on Aurora B kinase substrate phosphorylation. This leads to microtubule detachments, which in turn activates the SAC[1-3].

Meiotic divisions in mammalian oocytes are highly error prone, with severe consequences for fertility and health of the offspring[4, 5]. Correct attachment of chromosomes in meiosis I leads to the generation of stretched bivalents, but -unlike mitosis- not to tension between sister kinetochores, which co-orient. Here, we set out to address whether reduction of tension applied by the spindle on bioriented bivalents activates error correction, and as a consequence, the SAC. Treatment of oocytes in late prometaphase I with Eg5 kinesin inhibitor affects spindle tension but not attachments, as we show here using an optimized protocol for confocal imaging. After Eg5 inhibition, bivalents are correctly aligned but less stretched and as a result, Aurora B/C-dependent error correction with microtubule detachment takes place. This loss of attachments leads to SAC activation. Crucially, SAC activation itself does not require Aurora B/C kinase activity in oocytes.

Results

Whether attachment errors of mono-oriented kinetochore pairs that do not generate stretched bivalents, are recognized by Aurora B-dependent error correction in meiosis I was unknown. Aurora B and the closely related meiotic Aurora C kinase detach even correctly attached microtubule fibers during prometaphase of meiosis I[6], giving rise to the attachment and detachment cycles observed on kinetochore pairs by live-imaging[7]. Therefore, it was proposed that error correction has to be turned off progressively as oocytes continue from prometaphase into metaphase I, to allow establishment of stable end-on attachments[6]. Given the importance of Aurora B-dependent error correction for fidelity of the mitotic cell division[8] and the high error rate of meiosis I in oocytes[4, 5], we decided to clarify a potential role for Aurora B/C and error correction in mouse oocyte metaphase I.

We tested different drugs that have been used in mitosis to reduce tension to study error correction and subsequent SAC activation (see[2, 3, 9] for excellent reviews on SAC activation and tension in mitosis), in mouse oocytes. Our aim was to create a situation where bivalents are correctly attached, but under less stretch, in late prometaphase I (**Figure S1A**). The SAC protein Mad2 is recruited to unattached kinetochores early in prometaphase, and most Mad2 staining disappears by 4 hours after Germinal Vesicle Breakdown (GVBD), when stable attachments are formed[7, 10, 11]. Anaphase I takes place 7 to 9 hours after GVBD in the mouse strain we are using here. Oocytes were exposed to increasing concentrations of Taxol, Monastrol, or STLC (s-trityl-l-cysteine) 5 hours after GVBD -when bivalents are attached and aligned- for one hour. Taxol leads to the hyperstabilization of microtubule fibers which reduces pulling forces on kinetochores[12]. Monastrol[13, 14] and STLC[15-17] are inhibitors of the kinesin Eg5, which crosslinks anti-parallel microtubules [18]. Before fixation in metaphase I, oocytes were subjected to a short cold treatment to visualize only stable fibers, such as those attached to kinetochores[19]. In Taxol-treated oocytes, hyperstabilization of microtubule fibers was observed at all concentrations tested (**Figure S1B**), interfering with proper examination of kinetochore-attachment status such as described below. As expected, high concentrations of Monastrol and STLC resulted in collapsed monopolar spindles. Lower concentrations of both drugs allowed oocytes to maintain bipolar spindles with stable microtubule fibers (**Figure S1B**). Compared to Monastrol, treatment with STLC resulted in highly reproducible changes in spindle morphology at different concentrations, therefore we used STLC for subsequent experiments, and confirmed results with Taxol, were indicated.

Bivalents that are not attached to both poles cannot be maintained at the metaphase plate and move towards the poles, a phenotype observed in oocytes that are defective in stabilizing kinetochore fibers,

such as oocytes devoid of BubR1[19-21]. Addition of low concentrations of STLC in late prometaphase did not perturb alignment of bivalents, indicating that bivalents were still attached to the bipolar spindle (**Figure 1A**). Spindles did not show any obvious defects, apart from being significantly shorter than spindles of untreated oocytes. Importantly, bivalents were under less stretch, as determined by measuring the distance between pairs of sister kinetochores from each bivalent, in the number of oocytes indicated (**Figure 1B**). Similar phenotypes (chromosomes aligned, decreased interkinetochore distances) were observed with low doses of Taxol (**Figure 1C**).

To address whether error correction takes place in STLC-treated oocytes we characterized kinetochore-microtubule attachments with optimized confocal image acquisitions, followed by deconvolution[22]. Kinetochore pairs of cold-treated oocytes with or without STLC treatment were analysed and the percentage of end-on correct amphitelic, merotelic (mono-oriented sister kinetochores attached to both poles), and lateral interactions (kinetochores interact with the lateral side of the microtubule) was determined (**Figure 2A and S2A**). All kinetochores were interacting with microtubules in STLC-treated oocytes, as well as in control oocytes, but the frequency of merotelic attachments and lateral interactions increased from 3,5% in controls to more than 20% (**Figure 2A and B, Figure S2B**). STLC-treated oocytes harboured additionally interpolar fibers (**Figure 2B**). In short, bivalents were under less stretch in the presence of STLC, and a significant fraction of kinetochores formed merotelic or lateral interactions with microtubule fibers. In human somatic cells, Aurora B kinase activity allows establishment of lateral interactions when end-on attachments are destabilized[23]. Lateral interactions we observed in STLC-treated oocytes may therefore indicate ongoing error correction. Alternatively though, STLC-treatment itself may lead to loss of end-on amphitelic attachments.

If ongoing error correction and not STLC treatment itself were the reason for the presence of aberrant attachments/ interactions, inhibition of error correction by inhibiting Aurora B/C kinase should revert the phenotype. To inhibit Aurora B/C kinase we used the drug ZM447439, which mimics loss of both Aurora B and C in oocytes[24] with accelerated anaphase I onset, defects in cytokinesis, and a failure to extrude Polar Bodies (PBs). We controlled for efficient inhibition of Aurora B/C kinase by staining for Histone H3 phosphorylation on Serine 28, a prominent substrate of Aurora B/C, which becomes phosphorylated at GVBD[6] (**Figure S3A**). We also ruled out the concomitant inhibition of Aurora A by staining for phosphorylated Threonine 288, a read-out of active Aurora A in oocytes[25] (**Figure S3B**). Even though ZM447439 does not allow us to distinguish between Aurora B and C, it can be used to inhibit both kinases in oocytes.

To inhibit error correction in STLC-treated oocytes, we added ZM447439 prior to STLC treatment, and visualized cold-stable microtubule fibers. Indeed, the ratio of merotelic attachments/lateral interactions dropped to a value around 6%, similar to controls (**Figure 2A, S2A and B)**. Overlays of whole spindles showed stable end-on attachments in control and ZM447439-STLC-treated oocytes (**Figure 2B**). This indicates that without Aurora B/C, STLC treated oocytes maintain end-on attachments comparable to untreated oocytes. We conclude that aberrant attachments observed in STLC are due to ongoing error correction by Aurora B/C, and not STLC treatment *per se*.

Aurora B-dependent phosphorylation of several kinetochore substrates is required for error correction[8]. We analyzed Aurora B/C-dependent phosphorylation of Hec1 on S55 with a phospho-specific antibody[26], to determine whether ongoing error correction occurred in STLC-treated oocytes. An increase in Hec1 phosphorylation was observed upon STLC treatment, in accordance with kinetochores undergoing error correction. Crucially, this increase was dependent on Aurora B/C (**Figure 2C**).

Next we asked whether ongoing error correction had an effect on cell cycle progression in oocytes. Error correction activates the SAC in mitosis, presumably because unattached kinetochores are created. Lateral interactions which occur upon error correction[27], do not satisfy the SAC in mammalian somatic cells[28]. When the SAC is active, checkpoint proteins such as Mad2 are recruited to unattached kinetochores, to prevent APC/C-dependent ubiquitination and therefore proteasome-dependent degradation of Cyclin B1 and Securin, and anaphase onset[29]. The meiotic SAC is less stringent than in mitosis, inducing a cell cycle arrest only in the presence of several unattached kinetochores[4]. Hence, we were wondering whether ongoing error correction in oocytes created a signal strong enough for a detectable SAC-dependent cell cycle delay. Because loss of Aurora B/C leads to cytokinesis defects[24], we used degradation of exogenously expressed YFP-tagged Securin (and not anaphase onset and PB extrusion) as a read-out for SAC inactivation in live oocytes[30].

Securin-YFP was stabilized for several hours in STLC-treated oocytes, indicating that the SAC was indeed activated (**Figure 3A**). Accordingly, Mad2 was recruited to kinetochores at low levels upon STLC treatment (**Figure 3B**). If the delay in Securin-YFP degradation upon STLC treatment was indeed due to SAC activation, concomitantly inhibiting SAC function should abolish the delay. We added the well-characterized drug Reversine to inhibit the essential SAC kinase Mps1[19, 31, 32] and effectively rescued Securin-YFP degradation in STLC-treated oocytes (**Figure 3A**). A SAC response was also observed in Taxol-treated oocytes, albeit only within a very small window of Taxol concentration, probably because there was either not enough Taxol to reduce stretch, or too much which lead to such a hyperstabilization of

microtubule fibers that they could not be destabilized by Aurora B/C anymore, similar to what has been suggested in mitosis[33] (**Figure S4A**).

If ongoing error correction was creating unattached kinetochores that activate the SAC, inhibition of Aurora B/C with ZM447439 should abrogate SAC response in STLC treated oocytes. This was indeed the case, and the STLC-induced delay in Securin-YFP degradation and Mad2 recruitment did not occur in ZM447439-treated oocytes (**Figure 3B**, **C**). Securin-YFP degradation took place slightly earlier in oocytes without Aurora B/C activity than in controls (**Figure 3B**). We addressed the possibility that accelerated progression through meiosis I may have resulted in loss of Mad2 from kinetochores. ZM447439-treated oocytes were maintained in metaphase I by inhibiting proteasome-dependent degradation of Cyclin B1 and Securin with MG132[34]. Again, Mad2 was recruited to kinetochores in response to STLC, in an Aurora B/C-dependent manner (**Figure S4B**). These results indicate that less stretched bivalents activate Aurora B/C-dependent error correction. Transient microtubule detachment and formation of lateral interactions may then lead to SAC activation. Alternatively though, Aurora B/C may be required for a functional SAC, and SAC activation in STLC-treated oocytes may take place independently of error correction.

To distinguish between these two possibilities, we asked whether SAC response *per se* requires Aurora B/C kinase activity in oocytes. Whether Aurora B is essential for initial SAC activation is still controversial, and Aurora B kinase activity plays a role in prolonged SAC arrest in mitosis[35-38]. As shown before[11, 39], treatment of oocytes in late prometaphase, when bivalents are stably attached and under stretch, with low doses of the spindle-depolymerizing drug Nocodazole, led to a cell cycle delay. Stabilization of Securin-YFP and strong recruitment of Mad2 to kinetochores was observed (**Figure 4A and B**). To address whether Aurora B/C kinase is required for this SAC response, we added ZM447439 before treating oocytes with Nocodazole, and checked for Securin-YFP degradation. Importantly, inhibiting Aurora B/C did not suppress SAC response to Nocodazole (**Figure 4A**). We considered the possibility that Aurora B/C was not completely inhibited at the time we added Nocodazole, even though this was unlikely, given the fact that the same treatment interferred with error correction and a SAC-mediated delay in STLC treated oocytes (**Figure 3A-C**). But SAC response was efficient also upon longer exposure to ZM447439 prior to Nocodazole addition (**Figure S4C**). Hence, unattached kinetochores delay Securin-YFP degradation in an Aurora B/C-independent manner. Accordingly, strong recruitment of Mad2 to kinetochores was observed upon addition of Nocodazole, independently of whether Aurora B/C was active (**Figure 4B**), and also independently of MG132 induced metaphase I arrest (**Figure S4D**). Nevertheless, SAC-dependent stabilization of Securin-YFP was less robust in the presence of ZM447439,

suggesting that Aurora B/C is indeed required for maintaining prolonged SAC arrest, probably by preventing removal of SAC proteins, such as suggested in mitosis[36, 40] (**Figure 4A**). We conclude that Aurora B/C kinase activity is not essential for SAC activation in oocytes. Importantly, these results strongly suggest that missing bivalent stretch leads to the activation of error correction, and this indirectly leads to SAC activation and the observed cell cycle delay.

Discussion

We have established conditions to study response to correctly aligned and attached bivalents, which are not under tension and therefore not stretched, in oocytes. We show that Aurora B/C plays an important role in detecting whether bivalents are stretched in late prometaphase. Significant improvements in microtubule visualization by confocal microscopy[22] and high temporal resolution of meiotic maturation allowed us to detect error correction after end-on attachments have been formed, in late prometaphase. Our data fit with the recent model in mitosis that the SAC *per se* is satisfied by attachments and not tension applied on kinetochores[2, 3, 41-44]. We propose that in oocytes, Aurora B/C's role is essential for destabilization of microtubule fibers that do not generate stretched bivalents, to activate the SAC (**Figure 4C**). Therefore, even though in early meiosis Aurora B/C seemingly indiscriminately destabilizes all attachments[6], Aurora B/C becomes important as oocytes progress into metaphase to detect bivalents that are less stretched. Inhibition of Aurora B/C activity early in meiosis may indeed help oocytes establish stable attachments earlier[6], but we propose that Aurora B/C function is still important in late prometaphase, for detecting tension-less attachments.

Aurora B/C substrate phosphorylation decreases independently of bivalent stretching during progression through prometaphase I[6]. This was proposed to be mediated by increasing PP2A recruitment to kinetochores where it may counteract Aurora B/C[6]. Nevertheless, phosphorylation of two known Aurora B/C substrates, Hec1 and Knl1, remains high throughout oocyte meiotic maturation, even when bivalents are correctly attached[6, 45]. Inhibition of Aurora B/C does not lead to complete loss of Hec1 and Knl1 phosphorylation (this study, and [6]), and suggests that PP2A activity to counterbalance Aurora B/C substrate phosphorylation is not very efficient in oocytes. In mitosis, BubR1-dependent recruitment of PP2A counterbalances Aurora B/C phosphorylation to allow establishment of microtubule-kinetochore interactions[46-48]. It will be important to determine if there is a fraction of PP2A localized in the kinetochore region that is required for stabilization of kinetochore fibers, and to distinguish it from PP2A in the centromere region that brings about protection of cohesin in meiosis I[49]. Intriguingly, we have previously found that stabilization of microtubule-kinetochore interactions does not require BubR1

kinetochore localisation in oocytes, suggesting that error correction is shut off by means other than PP2A kinetochore-recruitment through BubR1[19]. Indeed, merotelic attachments are also observed in oocytes devoid of PP2A[45], indicating that Aurora B/C activity does not prevent the establishment of new attachments in oocyte meiosis. We hypothesize that a distinct, meiosis-specific mechanism to counteract Aurora B/C activity in the cytoplasm and not at kinetochores may permit establishment of end-on merotelic attachments during error correction. In conclusion, we show here for the first time that tension-less bivalents induce error correction in meiosis. Future work will address the physiological significance of error correction to prevent aneuploidies in mammalian oocytes, and the relevance of our results for error correction and SAC control in mitotic cells.

Author Contributions:

A.V., I.L., and E.B. performed most of the experiments with technical help from D.C., W.E.Y. was supervising I.L. with statistical analysis and chromosome spreads. S.B. and D.C. developed the workflow for high-resolution confocal imaging and performed acquisitions. E. B. supervised A.V. and I.L., and took part in the conceptualization of this study with K.W. Overall supervision, funding acquisition and project administration was done by K.W. Figures were prepared by A.V. and E.B., and the manuscript was written by K.W., with participation from E.B. and A.V., and input from all authors.

Acknowledgements

We thank Ian Cheeseman for reagents, Elvira Nikalayevich, Leonor Keating, and Aude Dupre for comments on the manuscript, lab members for suggestions and discussion, and administrative services and animal facility for support. A.V. received a PhD fellowship from the French Ministère de la Recherche, W.E.Y. a postdoctoral fellowship from ARC (Association de la Recherche sur le Cancer), and I.L. obtained support in part by an ERASMUS fellowship. The IBPS-imaging facility was supported by the Conseil Regional Ile-de-France. This study furthermore received support by the Agence Nationale de la Recherche (Subvention ANR-12-BSV2-0005-01, ANR-16-CE92-0007-01), and the Fondation de la Recherche Médicale (Equipe DEQ20160334921) to K.W., as well as core funding by UPMC and the CNRS, and Action Initiative (IBPS) to K.W. and S.B.

References

1. London, N., and Biggins, S. (2014). Signalling dynamics in the spindle checkpoint response. Nature reviews. Molecular cell biology *15*, 736-747.
2. Khodjakov, A., and Pines, J. (2010). Centromere tension: a divisive issue. Nature cell biology *12*, 919-923.
3. Etemad, B., Kuijt, T.E., and Kops, G.J. (2015). Kinetochore-microtubule attachment is sufficient to satisfy the human spindle assembly checkpoint. Nature communications *6*, 8987.
4. Touati, S.A., and Wassmann, K. (2016). How oocytes try to get it right: spindle checkpoint control in meiosis. Chromosoma *125*, 321-335.
5. Herbert, M., Kalleas, D., Cooney, D., Lamb, M., and Lister, L. (2015). Meiosis and Maternal Aging: Insights from Aneuploid Oocytes and Trisomy Births. Cold Spring Harb Perspect Biol *7*.
6. Yoshida, S., Kaido, M., and Kitajima, T.S. (2015). Inherent Instability of Correct Kinetochore-Microtubule Attachments during Meiosis I in Oocytes. Developmental cell *33*, 589-602.
7. Kitajima, T.S., Ohsugi, M., and Ellenberg, J. (2011). Complete kinetochore tracking reveals error-prone homologous chromosome biorientation in mammalian oocytes. Cell *146*, 568-581.
8. van der Waal, M.S., Hengeveld, R.C., van der Horst, A., and Lens, S.M. (2012). Cell division control by the Chromosomal Passenger Complex. Experimental cell research *318*, 1407-1420.
9. Nezi, L., and Musacchio, A. (2009). Sister chromatid tension and the spindle assembly checkpoint. Curr Opin Cell Biol *21*, 785-795.
10. Hached, K., Xie, S.Z., Buffin, E., Cladiere, D., Rachez, C., Sacras, M., Sorger, P.K., and Wassmann, K. (2011). Mps1 at kinetochores is essential for female mouse meiosis I. Development *138*, 2261-2271.
11. Wassmann, K., Niault, T., and Maro, B. (2003). Metaphase I Arrest upon Activation of the Mad2-Dependent Spindle Checkpoint in Mouse Oocytes. Curr Biol *13*, 1596-1608.
12. Jordan, M.A., Toso, R.J., Thrower, D., and Wilson, L. (1993). Mechanism of mitotic block and inhibition of cell proliferation by taxol at low concentrations. Proceedings of the National Academy of Sciences of the United States of America *90*, 9552-9556.
13. Mayer, T.U., Kapoor, T.M., Haggarty, S.J., King, R.W., Schreiber, S.L., and Mitchison, T.J. (1999). Small molecule inhibitor of mitotic spindle bipolarity identified in a phenotype-based screen. Science *286*, 971-974.
14. Kapoor, T.M., Mayer, T.U., Coughlin, M.L., and Mitchison, T.J. (2000). Probing spindle assembly mechanisms with monastrol, a small molecule inhibitor of the mitotic kinesin, Eg5. The Journal of cell biology *150*, 975-988.
15. Paull, K.D., Lin, C.M., Malspeis, L., and Hamel, E. (1992). Identification of novel antimitotic agents acting at the tubulin level by computer-assisted evaluation of differential cytotoxicity data. Cancer Res *52*, 3892-3900.
16. Brier, S., Lemaire, D., Debonis, S., Forest, E., and Kozielski, F. (2004). Identification of the protein binding region of S-trityl-L-cysteine, a new potent inhibitor of the mitotic kinesin Eg5. Biochemistry *43*, 13072-13082.
17. Skoufias, D.A., DeBonis, S., Saoudi, Y., Lebeau, L., Crevel, I., Cross, R., Wade, R.H., Hackney, D., and Kozielski, F. (2006). S-trityl-L-cysteine is a reversible, tight binding

inhibitor of the human kinesin Eg5 that specifically blocks mitotic progression. The Journal of biological chemistry *281*, 17559-17569.
18. Valentine, M.T., Fordyce, P.M., and Block, S.M. (2006). Eg5 steps it up! Cell division *1*, 31.
19. Touati, S.A., Buffin, E., Cladiere, D., Hached, K., Rachez, C., van Deursen, J.M., and Wassmann, K. (2015). Mouse oocytes depend on BubR1 for proper chromosome segregation but not for prophase I arrest. Nature communications *6*, 6946.
20. Homer, H., Gui, L., and Carroll, J. (2009). A spindle assembly checkpoint protein functions in prophase I arrest and prometaphase progression. Science *326*, 991-994.
21. Wei, L., Liang, X.W., Zhang, Q.H., Li, M., Yuan, J., Li, S., Sun, S.C., Ouyang, Y.C., Schatten, H., and Sun, Q.Y. (2009). BubR1 is a spindle assembly checkpoint protein regulating meiotic cell cycle progression of mouse oocyte. Cell cycle *Georgetown*, 1112-1121.
22. Lam, F., Cladiere, D., Guillaume, C., Wassmann, K., and Bolte, S. (2017). Super-resolution for everybody: An image processing workflow to obtain high-resolution images with a standard confocal microscope. Methods *115*, 17-27.
23. Shrestha, R.L., Conti, D., Tamura, N., Braun, D., Ramalingam, R.A., Cieslinski, K., Ries, J., and Draviam, V.M. (2017). Aurora-B kinase pathway controls the lateral to end-on conversion of kinetochore-microtubule attachments in human cells. Nature communications *8*, 150.
24. Balboula, A.Z., and Schindler, K. (2014). Selective disruption of aurora C kinase reveals distinct functions from aurora B kinase during meiosis in mouse oocytes. PLoS genetics *10*, e1004194.
25. Chmatal, L., Yang, K., Schultz, R.M., and Lampson, M.A. (2015). Spatial Regulation of Kinetochore Microtubule Attachments by Destabilization at Spindle Poles in Meiosis I. Curr Biol *25*, 1835-1841.
26. Welburn, J.P., Vleugel, M., Liu, D., Yates, J.R., 3rd, Lampson, M.A., Fukagawa, T., and Cheeseman, I.M. (2010). Aurora B phosphorylates spatially distinct targets to differentially regulate the kinetochore-microtubule interface. Mol Cell *38*, 383-392.
27. Kalantzaki, M., Kitamura, E., Zhang, T., Mino, A., Novak, B., and Tanaka, T.U. (2015). Kinetochore-microtubule error correction is driven by differentially regulated interaction modes. Nature cell biology *17*, 530.
28. Kuhn, J., and Dumont, S. (2017). Spindle assembly checkpoint satisfaction occurs via end-on but not lateral attachments under tension. The Journal of cell biology.
29. Lischetti, T., and Nilsson, J. (2015). Regulation of mitotic progression by the spindle assembly checkpoint. Mol Cell Oncol *2*, e970484.
30. Herbert, M., Levasseur, M., Homer, H., Yallop, K., Murdoch, A., and McDougall, A. (2003). Homologue disjunction in mouse oocytes requires proteolysis of securin and cyclin B1. Nature cell biology *5*, 1023-1025.
31. El Yakoubi, W., Buffin, E., Cladière, D., Gryaznova, Y., Berenguer, I., Touati, A.S., Gomez, R., Suja, J.A., van Deursen, J.M., and Wassmann, K. (2017). Mps1 kinase-dependent Sgo2 centromere localisation mediates cohesin protection in mouse oocyte meiosis I. Nature communications.
32. Santaguida, S., Tighe, A., D'Alise, A.M., Taylor, S.S., and Musacchio, A. (2010). Dissecting the role of MPS1 in chromosome biorientation and the spindle checkpoint through the small molecule inhibitor reversine. The Journal of cell biology *190*, 73-87.

33. Yang, Z., Kenny, A.E., Brito, D.A., and Rieder, C.L. (2009). Cells satisfy the mitotic checkpoint in Taxol, and do so faster in concentrations that stabilize syntelic attachments. The Journal of cell biology *186*, 675-684.
34. Terret, M.E., Wassmann, K., Waizenegger, I., Maro, B., Peters, J.M., and Verlhac, M.H. (2003). The Meiosis I-to-Meiosis II Transition in Mouse Oocytes Requires Separase Activity. Curr Biol *13*, 1797-1802.
35. Santaguida, S., Vernieri, C., Villa, F., Ciliberto, A., and Musacchio, A. (2011). Evidence that Aurora B is implicated in spindle checkpoint signalling independently of error correction. The EMBO journal *30*, 1508-1519.
36. Gurden, M.D., Anderhub, S.J., Faisal, A., and Linardopoulos, S. (2016). Aurora B prevents premature removal of spindle assembly checkpoint proteins from the kinetochore: A key role for Aurora B in mitosis. Oncotarget.
37. Kallio, M.J., McCleland, M.L., Stukenberg, P.T., and Gorbsky, G.J. (2002). Inhibition of aurora B kinase blocks chromosome segregation, overrides the spindle checkpoint, and perturbs microtubule dynamics in mitosis. Curr Biol *12*, 900-905.
38. Vader, G., Cruijsen, C.W., van Harn, T., Vromans, M.J., Medema, R.H., and Lens, S.M. (2007). The chromosomal passenger complex controls spindle checkpoint function independent from its role in correcting microtubule kinetochore interactions. Molecular biology of the cell *18*, 4553-4564.
39. Homer, H.A., McDougall, A., Levasseur, M., Murdoch, A.P., and Herbert, M. (2005). Mad2 is required for inhibiting securin and cyclin B degradation following spindle depolymerisation in meiosis I mouse oocytes. Reproduction *130*, 829-843.
40. Famulski, J.K., and Chan, G.K. (2007). Aurora B kinase-dependent recruitment of hZW10 and hROD to tensionless kinetochores. Curr Biol *17*, 2143-2149.
41. Tauchman, E.C., Boehm, F.J., and DeLuca, J.G. (2015). Stable kinetochore-microtubule attachment is sufficient to silence the spindle assembly checkpoint in human cells. Nature communications *6*, 10036.
42. Magidson, V., He, J., Ault, J.G., O'Connell, C.B., Yang, N., Tikhonenko, I., McEwen, B.F., Sui, H., and Khodjakov, A. (2016). Unattached kinetochores rather than intrakinetochore tension arrest mitosis in taxol-treated cells. The Journal of cell biology *212*, 307-319.
43. Pinsky, B.A., Kung, C., Shokat, K.M., and Biggins, S. (2006). The Ipl1-Aurora protein kinase activates the spindle checkpoint by creating unattached kinetochores. Nature cell biology *8*, 78-83.
44. Pinsky, B.A., and Biggins, S. (2005). The spindle checkpoint: tension versus attachment. Trends Cell Biol *15*, 486-493.
45. Tang, A., Shi, P., Song, A., Zou, D., Zhou, Y., Gu, P., Huang, Z., Wang, Q., Lin, Z., and Gao, X. (2016). PP2A regulates kinetochore-microtubule attachment during meiosis I in oocyte. Cell cycle *15*, 1450-1461.
46. Suijkerbuijk, S.J., Vleugel, M., Teixeira, A., and Kops, G.J. (2012). Integration of kinase and phosphatase activities by BUBR1 ensures formation of stable kinetochore-microtubule attachments. Developmental cell *23*, 745-755.
47. Kruse, T., Zhang, G., Larsen, M.S., Lischetti, T., Streicher, W., Kragh Nielsen, T., Bjorn, S.P., and Nilsson, J. (2013). Direct binding between BubR1 and B56-PP2A phosphatase complexes regulate mitotic progression. Journal of cell science *126*, 1086-1092.

48. Xu, P., Raetz, E.A., Kitagawa, M., Virshup, D.M., and Lee, S.H. (2013). BUBR1 recruits PP2A via the B56 family of targeting subunits to promote chromosome congression. Biol Open *2*, 479-486.
49. Gutierrez-Caballero, C., Cebollero, L.R., and Pendas, A.M. (2012). Shugoshins: from protectors of cohesion to versatile adaptors at the centromere. Trends in genetics : TIG *28*, 351-360.
50. Niault, T., Hached, K., Sotillo, R., Sorger, P.K., Maro, B., Benezra, R., and Wassmann, K. (2007). Changing Mad2 levels affects chromosome segregation and spindle assembly checkpoint control in female mouse meiosis I. PloS one *2*, e1165.
51. Chambon, J.P., Hached, K., and Wassmann, K. (2013). Chromosome spreads with centromere staining in mouse oocytes. Methods Mol Biol *957*, 203-212.
52. Wassmann, K., and Benezra, R. (1998). Mad2 transiently associates with an APC/p55Cdc complex during mitosis. Proceedings of the National Academy of Sciences of the United States of America *95*, 11193-11198.

Figure Legends

Figure 1

Addition of STLC and Taxol reduces chromosome stretch.

(A-C) Whole-mount immunofluorescence staining of cold-treated spindles from oocytes fixed 6 hours after GVBD. Microtubules were stained with anti-Tubulin antibody (green), kinetochores with CREST (red) and chromosomes with Hoechst (blue). Where indicated, oocytes were treated 5 hours after GVBD with STLC (0.75µM) (A,B) or with Taxol (1µM) (C). (A) Overlays of z-sections covering the whole volume of the spindle (15 to 25µm) are shown. Scale bar: 5µm. Any chromosome that was at least partially in the pole region was scored as unaligned. The relative frequency of well-aligned (0 unaligned chromosomes), mild alignment defects (1-2 unaligned chromosomes) and strong alignment defects (3 or more unaligned chromosomes, none detected) per oocyte is shown (n: number of oocytes). Three independent experiments involving a total of at least 3 mice have been performed. (B) Partial overlays from the same oocyte as in (A) are shown to observe each chromosome individually. Scale bar: 5µm. Magnifications of a stretched and a less stretched chromosome are shown in the insets. Scale bar: 2µm. The graphs on the right show the distribution of spindle length values (n: number of oocytes) and of interkinetochore distances (n: number of bivalents). Three independent experiments involving a total of at least 3 mice have been performed. Interkinetochore distances were determined as indicated in the magnifications. (C) Partial overlays to observe chromosomes individually. Scale bar: 5µm. Magnifications of a fully stretched chromosome and a less stretched chromosome are shown in the insets. Scale bar: 2µm. Interkinetochore distances were determined as indicated in the magnifications. On the right, the distribution of interkinetochore distances is shown (n: number of bivalents). Two independent experiments involving a total of at least 2 mice have been performed. Mean and standard deviation are indicated. Two-tailed unpaired Student's t-test was performed for statistical test (not significant [ns] p value >0,05, *** p value < 0.0001). Related to Figure S1.

Figure 2

Destabilization of kinetochore-microtubule fibers under reduced tension requires Aurora B/C.

(A) The table on the left shows examples of end-on amphitelic, merotelic and lateral microtubule attachments/interactions observed in spindle stainings in (B). Scale bar: 2µm. The percentage per oocyte of amphitelic end-on attachments, or merotelic attachments and lateral interactions is indicated, for each condition. The graph on the right shows the distribution of the percentage per oocyte of merotelic/lateral attachments/ interactions. Error bars are standard error of the mean. Where indicated, oocytes were treated either with STLC (0.75µM) at 5 hours after GVBD, or additionally with ZM447439 (10µM) 15 minutes

prior to STLC treatment. n: number of oocytes, 3 independent experiments involving a total of at least 6 mice have been performed. Two-tailed unpaired Student's t-test was performed (not significant [ns] p value= 0.21, *** p value < 0.0001). **(B)** Whole-mount immunofluorescence staining of cold-treated spindles from oocytes fixed at 6 hours after GVBD. Spindles were imaged with a confocal microscope, using a workflow enabling near super-resolution pictures. Microtubule fibers were stained with anti-Tubulin antibody (green), kinetochores with CREST (red) and chromosomes with Hoechst (blue). Representative images of oocytes analyzed in (A) are shown as 3D reconstructions. n: number of oocytes, 3 independent experiments involving a total of at least 6 mice have been performed. Scale bar: 5µm. **(C)** Chromosome spreads of metaphase I oocytes. Oocytes were treated with the drug ZM447439 (10µM) 15 minutes prior to STLC treatment (0.75µM) at 5 hours after GVBD, where indicated. Chromosomes were stained with Hoechst (blue), CREST (green) and anti-Hec1pS55 (red) antibodies. Scale bar: 2µm. n: number of oocytes. On the right, the distribution of Hec1pS55 signal intensity normalized to CREST and relative to the control mean for each experiment is shown. The values corresponding to all kinetochores measured are displayed (n: number of kinetochores). Statistical analysis was performed on the mean value calculated for each oocyte from 3 independent experiments involving a total of at least 4 mice. Mean and standard deviation of the whole population are shown. p values were calculated with two-tailed unpaired Student's t-test (not significant [ns] p value > 0.05, ***p value < 0.0001). Related to Figure S2 and S3.

Figure 3

STLC treatment leads to SAC activation in an Aurora B/C-dependent manner.

(A) Oocytes were injected with Securin-YFP encoding mRNA at GV stage. Securin-YFP signal intensity was monitored by time-lapse fluorescence imaging and normalized to the highest value for each oocyte. Mean and standard deviation of the population are plotted in arbitrary units against time. As indicated in the scheme on the right, oocytes were treated with STLC (0.75µM) at 5 hours after GVBD and with Reversine (0.5µM) at 5.5 hours after GVBD. n: number of oocytes. At least two independent experiments involving a total of at least 6 mice have been performed. **(B)** Chromosome spreads of metaphase I oocytes. Oocytes were treated with the drug ZM447439 (10µM) 15 minutes prior to STLC treatment (0.75µM) at 5 hours after GVBD, where indicated, as shown on the scheme on the right. Chromosomes were stained with Hoechst (blue), CREST (green) and anti-Mad2 (red) antibodies. Scale bar: 5µm. n: number of oocytes. On the right, the distribution of Mad2 signal intensity relative to CREST is shown. The values corresponding to all kinetochores measured are displayed (n: number of kinetochores). Statistical analysis was performed on the mean value calculated for each oocyte from 3 independent experiments involving a total of at least 6 mice. Mean and standard deviation of the whole population are shown. p values were calculated with two-tailed unpaired Student's t-test (not significant [ns] p value > 0.05, ***p value <

0.0001). **(C)** Oocytes were injected with Securin-YFP encoding mRNA at GV stage as desribed in (A). As indicated on the scheme in (B), oocytes were treated with ZM447439 (10µM) 4 hours 45 minutes after GVBD, and with STLC (0.75µM) 5 hours after GVBD. n: number of oocytes. Four independent experiments involving a total of at least 8 mice have been performed.

Figure 4

SAC activation in response to missing attachments does not require Aurora B/C kinase activity in meiosis I.

(A) As indicated on the scheme on the right, oocytes were injected at GV stage with Securin-YFP encoding mRNA and treated with the drug ZM447439 (10µM) at 4 hours 45 minutes after GVBD, prior to Nocodazole treatment (400nM) at 5 hours after GVBD. YFP signal intensity was monitored by time-lapse fluorescence imaging and normalized to the highest value for each oocyte. n: number of oocytes. Mean and standard deviation of the population are plotted in arbitrary units against time. Two independent experiments involving a total of at least 4 mice have been performed. **(B)** Chromosome spreads of metaphase I oocytes (GVBD+6h). Where indicated, oocytes were treated with the drug ZM447439 (10µM) at 4 hours 45 minutes after GVBD, prior to Nocodazole treatment (400nM) at 5 hours after GVBD. Chromosomes were stained with Hoechst (blue), CREST (green) and anti-Mad2 antibodies (red). Scale bar: 5µm. n: number of oocytes. The graph on the right shows the distribution of Mad2 signal intensities normalized to CREST. The values corresponding to all kinetochores measured are displayed (n: number of kinetochores). Statistical analysis was performed on the mean value calculated for each oocyte. Three independent experiments involving a total of at least 6 mice have been performed. p values were calculated with two-tailed unpaired Student's t-test (not significant [ns] p value > 0.05, ***p value < 0.0001). Error bars show Standard Deviation. **(C)** Model illustrating that Aurora B/C kinase is required for the recognition of less stretched bivalents in metaphase I by creating unattached kinetochore that are recognized by the SAC, causing a delay in APC/C activation and anaphase I onset. KT-MT fibers: kinetochore-microtubule fibers. See text for details. Related to Figure S4.

Star Methods

CONTACT FOR REAGENT AND RESOURCE SHARING

Further information and requests for resources and reagents should be directed to and will be fulfilled by the Lead Contact, Katja Wassmann (katja.wassmann@upmc.fr).

EXPERIMENTAL MODEL AND SUBJECT DETAILS

Animals

Adult CD-1 mice were purchased from Janvier Lab, France, and maintained according to current French guidelines in the conventional mouse facility of UMR7622, under the authorization C 75-05-13. All experiments were subject to ethical review and approved by the French Ministry of Higher Education and Research (authorization n° B-75-1308). Mice were not genetically modified, or exposed to drug treatment. All mice used in this study were females that were purchased at 7 weeks of age, not used for breedings and used at 8-16 weeks of age for experiments. The mice had not been involved in any previous procedures. Mice were given *ad libitum* access to food and water supply and were housed under a 12 hour light / 12 hour dark cycle in a specific pathogen-free environnement according to the Federation of European Laboratory Science Associations (FELASA).

Oocyte collection and culture

Oocytes were harvested from CD-1 mice aged 8 to 16 weeks. Mice were killed by cervical dislocation and the dissected ovaries were transferred directly into home-made M2 medium at 38°C. Oocytes were isolated from follicular cells by careful mouth pipetting with torn-out Pasteur pipettes with a diameter not exceeding 80µm. For microinjection experiments, oocytes were kept at GV stage in commercial M2 medium (Sigma-Aldrich), supplemented with 100µg/ml dbcAMP (Sigma-Aldrich). Oocytes were cultured in petri dishes containing M2 drops covered with mineral oil (Sigma-Aldrich), to prevent evaporation. Oocytes undergoing GVBD within 90 minutes after ovary dissection or alternatively, release from dbcAMP containing medium, were collected. All manipulations involving oocytes were done on heating plates at 38°C.

METHOD DETAILS

Small molecule inhibitors

All drugs were added to home-made M2 medium at the indicated final concentrations. Nocodazole (Sigma-Aldrich) was used at a final concentration of 400nM, Taxol (Paclitaxel from Sigma-Aldrich) was

used at 1µM. For Eg5 inhibition, Monastrol (Sigma-Aldrich) was used at 35µM and 70µM, STLC (S-Trityl-L-cystein, Sigma-Aldrich) at 0.75µM and 1µM, as indicated. For Mps1 inhibition, Reversine (Calbiochem) was used at 0.5µM, and for Aurora B inhibition, ZM447439 (Tocris) at 10µM. MG132 (Z-LEU-LEU-LEU-AL, Sigma-Aldrich) was used at 20µM.

Microinjection and live imaging

Securin-YFP capped mRNA was obtained by *in vitro* transcription, using the T3 Ambion mMessage Machine kit[53]. 1 to 10pM of capped mRNA was purified on RNeasy purification columns from Qiagen. GV oocytes were microinjected on an inverted Nikon Eclipse Ti microscope with self-made micropipettes, and manipulated using a holding pipette (VacuTip from Eppendorf). The injection flow was controlled by a FemtoJet Microinjector pump (Eppendorf). Live imaging of oocytes was performed on a Nikon eclipse TE 2000-E inverted microscope with motorized stage, equipped with PrecisExite High Power LED Fluorescence (LAM 1: 400/465, LAM 2: 585), a temperature chamber (Life Imaging Services), a Märzhäuser Scanning Stage, a CoolSNAP HQ2 camera, and controlled by Metamorph software. Oocytes were maintained in a Ludin chamber (Roper Scientific). Images were taken using a Plan APO (20 x 0.75 NA) objective.

Immunofluorescence and chromosome spreads

The *zona pellucida* of oocytes was removed in successive baths in Tyrode's acid solution, and oocytes were left to recover[54]. For whole-mount immunofluorescence, oocytes were first transferred in chambers coated with Concanavaline A (Sigma-Aldrich) in M2 PVP (Polyvinylpyrrolidone from Merck-Millipore) medium, followed by centrifugation at 1400 rpm for 13 minutes, all at 38°C. Prior to fixation, oocytes were incubated in a cold treatment solution (0.08M PIPES, 1mM $MgCl_2$, pH 7.4) on top of an ice-water bath to maintain a temperature of 4°C for 4 minutes. Oocytes were then fixed in a formaldehyde solution (BRB80 medium with 0.3% Triton X-100, 1.9% formaldehyde (Sigma-Aldrich)) at 38°C. For chromosome spreads, oocytes were fixed in a spread solution (1% paraformaldehyde, 0.15% Triton X-100 and 3mM 1,4 Dithiothreitol, all from Sigma-Aldrich) at room temperature[54]. Antibody staining was done using the following antibodies at the indicated dilutions: human CREST serum autoimmune antibody against centromere (Immunovision, HCT-0100, 1:100), mouse monoclonal anti-alpha-tubulin (DM1A) coupled to FITC (Sigma-Aldrich, F2168, 1:100), rat monoclonal anti-H3pS28 (Abcam, #ab10543, 1:500), rabbit polyclonal anti-Aurora A pT288 (Novus Biologicals, #NB100-2371, 1:100), rabbit polyclonal anti-Hec1 pS55 (Genetex, #GTX70017, 1:200), and rabbit polyclonal anti-Mad2[55] (1:100). The following secondary antibodies were used: anti-human Alexa 488 (Life Technologies, A11013, 1:200), anti-human Cy3 (Jackson ImmunoResearch, #709-166-149, 1:200), and anti-rat Cy3 (Jackson ImmunoResearch,

#712-167-003, 1:200), and anti-rabbit Cy3 (Jackson ImmunoResearch, #711-166-152, 1:200). Chromosomes were stained with Hoechst 33342 (Invitrogen, H21492) at 50 μg/ml. AF1 (Cityfluor) mounting medium was used for all immunofluorescence stainings, except for the high-resolution acquisitions in which case AF was supplemented with 83% (w/w) of Methyl phenyl sulfoxid (Sigma-Aldrich) in order to match a refractive index of 1.518.

Image acquisition

Images of chromosome spreads and whole mount oocytes were acquired on a Zeiss spinning disk confocal microscope, using a 100X (1.4 Oil) objective coupled to an EMCCD camera (Evolve 512, Photometrics). 10 z-sections of 0.4μm were taken for spreads, and 20-25 z-sections of 1μm for whole mount oocytes. High-resolution kinetochore attachment acquisitions were performed on a Leica TCS SP5-II, using a Leica 63x oil immersion objective (HCX Plan AOI CS, 1.4 NA). 150-300 z-sections of 80nm were taken for acquisitions; the scanning speed was 400 Hz, with a pinhole aperture adjusted to 1 Airy unit or 0.6 Airy unit; immersion oil with a refractive index of 1.518 has been used; raw pictures were then deconvoluted with Huygens 3.7 software using the Point Spread Function (PSF) from fluorescent beads of 100nm. For detailed description of the optimised workflow see[22]. 3-D reconstitutions of whole mount oocytes in Figure 2B were obtained using Arivis 4D, all other stacks were assembled in Image J.

QUANTIFICATION AND STATISTICAL ANALYSIS

Quantification of fluorescence signal

For quantification of fluorescence signals at kinetochores (Mad2 and Hec1pS55), fluorescence intensity was calculated as follows: for each kinetochore, a 10 x 10 pixels square was manually placed at the middle of the kinetochore structure detected with the CREST signal. Another 10 x 10 pixels square was placed adjacent to the first square to measure the background signal. Mean values for each channel were measured and the background was substracted. Signal intensities were normalized to the CREST signal from the same kinetochore. For Aurora A pT288 and Histone H3 pS28 signal quantification, mean intensity was measured in each oocyte in a circle of 380 pixels including the two pools of staining present at both poles of the spindle for Aurora A pT288 or including all the chromosomes for H3 pS28. The average of the background measured in 3 circles of 180 pixels was calculated and the mean intensity was then substracted. All measurements were performed on maximum intensity Z-projections of stacks of the original, untreated acquisitions. For Securin-YFP quantifications, a square of 100 x 100 pixels was manually placed in the center of the oocyte, and for each condition, the average background signal was calculated from two 100 x 100 pixel squares. For each time point, the YFP-signal was measured, and the

average background signal was substracted. For each oocyte, values were normalized relative to the highest value of the time-lapse. Measurements were performed with ImageJ software.

Meiotic spindle measurements

For spindle length measurements as well as high-resolution acquisitions, only oocytes in which the spindle was parallel to the confocal plane were analysed. Metaphase I spindle length was measured on maximum intensity Z-projections of stacks using ImageJ line tool.

Statistical analysis

Statistical analysis was performed using Graphpad Prism 6 software. Graphs were generated using GraphPad Prism software. Student's t-tests were performed on unpaired data and were two-tailed (ns: not significant, * $p < 0.05$, ** $p < 0.001$, *** $p < 0.0001$). Error bars indicate means ± standard deviation unless otherwise specified. Sample size and statistical tests are indicated within the figures and figure legends. Selection of oocytes for different conditions was at random. The number of independent replicates (at least two) and the number of mice involved is indicated for each Figure. n designates the number of oocytes used, except in Figures S4B and D, and the graph in Figure 2C, 3B, and 4B, where n designated the number of kinetochore pairs analysed. No statistical analysis was used to determine sample size. Collection and analysis of the data were not performed blind to the conditions of the experiments, no data from experiments were excluded from analysis.

KEY RESOURCES TABLE

REAGENT or RESOURCE	SOURCE	IDENTIFIER
Antibodies		
Human CREST serum autoimmune antibody	Immunovision	Cat# HCT-0100
Mouse monoclonal anti-alpha-Tubulin (DM1A) coupled to FITC	Sigma-Aldrich	Cat# F2168 RRID: AB_476967
Rat monoclonal anti-H3pS28	Abcam	Cat# ab10543 RRID: AB_2295065
Rabbit polyclonal anti-Hec1 pS55	Genetex	Cat# GTX70017 RRID: AB_11162004
Rabbit polyclonal anti-Aurora A pT288	Novus Biologicals	Cat# NB100-2371 RRID: AB_577685
Rabbit polyclonal anti-Mad2	From the Lab [52]	N/A
Alexa Fluor 488 goat anti human IgG (H+L)	ThermoFischer	Cat# A-11013 RRID: AB_141360
Cy3 AffiniPure Fab Fragment Donkey anti-Rat IgG (H+L)	Jackson immunoresearch	Cat# 712-167-003 RRID: AB_2340670
Cy3 AffiniPure Fab Fragment Donkey anti-Rabbit (H+L)	Jackson immunoresearch	Cat# 711-166-152 RRID: AB_2313568
Cy3 AffiniPure Fab Fragment Donkey anti-Human (H+L)	Jackson immunoresearch	Cat# 709-166-149 RRID: AB_2340538
Chemicals, Peptides, and Recombinant Proteins		
M2 medium with HEPES, without penicillin and streptomycin	Sigma-Aldrich	Cat# M7167-50ML
EmbryoMax® Penicillin/Streptomicin, solution 100X	Merck	Cat# TMS-AB2-C
N^6,2′-O-Dibutyryladenosine 3′,5′-cyclic monophosphate sodium salt (dbcAmp)	Sigma-Aldrich	Cat# D0260-25MG CAS Number: 16980-9-5
Mineral Oil	Sigma-Aldrich	Cat# M5310 CAS Number: 8042-47-5
Polyvinylpyrrolidone (PVP)	Merck-Millipore	Cat# 5295-100G CAS Number: 9003-39-8
Concanavalin A	Sigma-Aldrich	Cat# C5275 CAS Number: 11028-71-0
AF1 Mounting Medium	CityFluor	Cat# E17970-25
Methyl phenyl sulfoxide	Sigma-Aldrich	Cat# 261696 CAS Number: 1193-82-4
Formaldehyde	Sigma-Aldrich	Cat# 252549 CAS Number: 50-00-0
Paraformaldehyde	Sigma-Aldrich	Cat# 441244 CAS Number: 30525-89-4
DL-Dithiothreitol (DTT)	Sigma-Aldrich	Cat# D9779 CAS Number: 3483-12-3

Nocodazole	Sigma-Aldrich	Cat# M1404-10MG CAS Number: 31430-18-9
STLC (S-Trityl-L-cystein)	Sigma-Aldrich	Cat# 164739-5G CAS Number: 2799-07-7
Monastrol	Sigma-Aldrich	Cat# 475879-1mg CAS Number: 254753-54-3
Taxol (Paclitaxel)	Sigma-Aldrich	Cat# T7191-1MG CAS Number: 33069-62-4
ZM447439	Biotechne (Tocris)	Cat# 2458 CAS Number: 331771-20-1
Reversine	Calbiochem	Cat# 554717-5MG CAS Number: 656820-32-5
MG132 (Z-LEU_LEU_LEU_AL)	Sigma-Aldrich	Cat# C2211-5MG CAS Number: 133407-82-6
Critical Commercial Assays		
mMESSAGE mMACHINE T3 Kit	Life technologies (Ambion)	Cat# AM1348
RNeasy Mini Kit	QIAGEN	Cat# 74104
Experimental Models: Organisms/Strains		
Mouse: SWISS CD-1	Janvier lab	RjOrl:SWISS
Recombinant DNA		
pRN3-Securine-YFP	[50]	N/A
Software and Algorithms		
ImageJ	NIH	https://imagej.net/Fiji/Downloads
Huygens 3.7	Scientific Volume Imaging	https://svi.nl/Huygens Professional
Graphpad Prism 6	Graphpad software	https://www.graphpad.com/scientific-software/prism/
Arivis vision 4D	Arivis	https://www.arivis.com/en

Figure 1

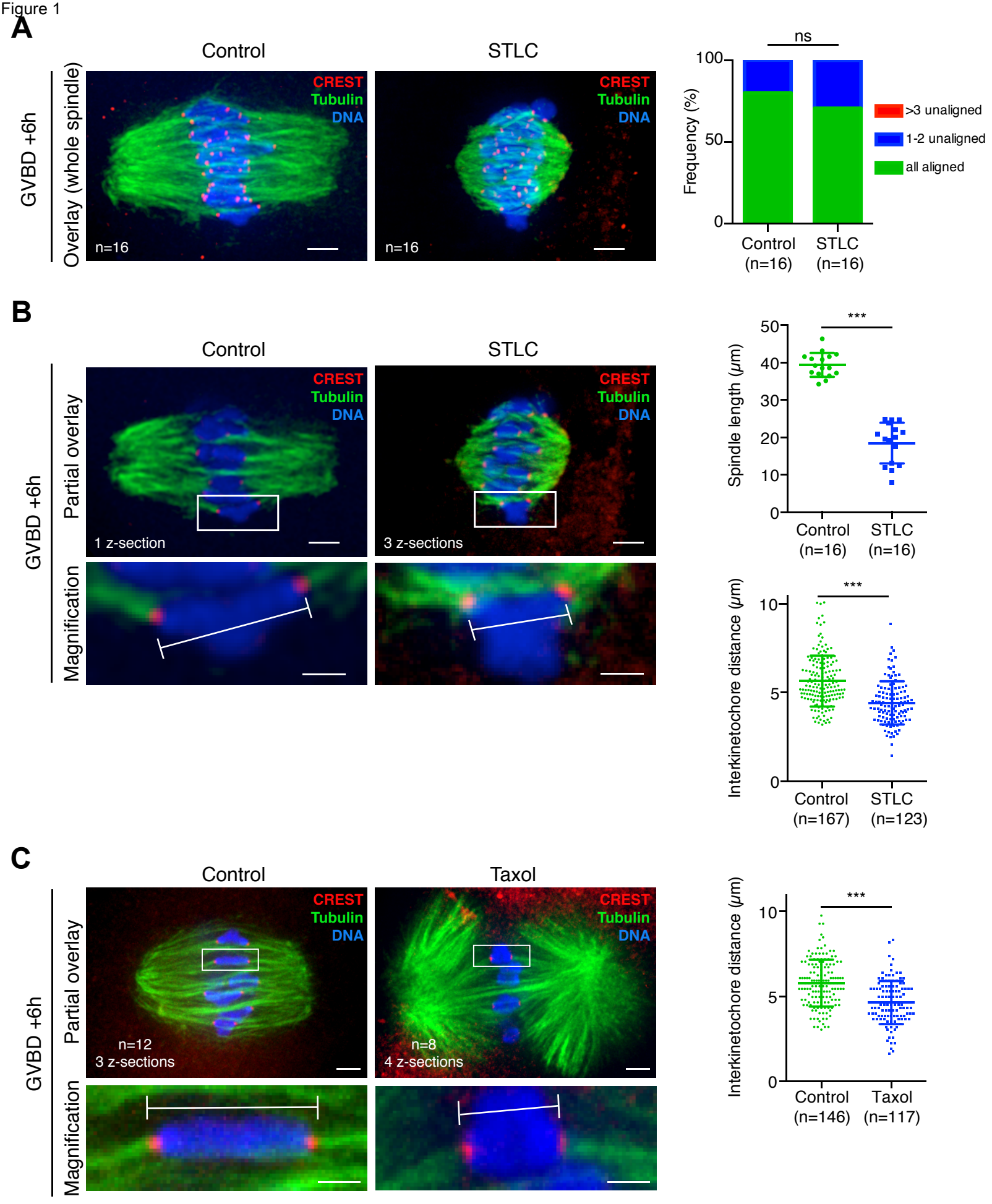
A
Control
STLC
GVBD +6h
Overlay (whole spindle)
CREST
Tubulin
DNA
n=16
n=16
ns
100
50
0
Frequency (%)
>3 unaligned
1-2 unaligned
all aligned
Control
(n=16)
STLC
(n=16)
B
Control
STLC
GVBD +6h
Partial overlay
Magnification
CREST
Tubulin
DNA
1 z-section
3 z-sections
***
50
40
30
20
10
0
Spindle length (μm)
Control
(n=16)
STLC
(n=16)
***
10
5
0
Interkinetochore distance (μm)
Control
(n=167)
STLC
(n=123)
C
Control
Taxol
GVBD +6h
Partial overlay
Magnification
CREST
Tubulin
DNA
n=12
3 z-sections
n=8
4 z-sections
***
10
5
0
Interkinetochore distance (μm)
Control
(n=146)
Taxol
(n=117)

Figure 2

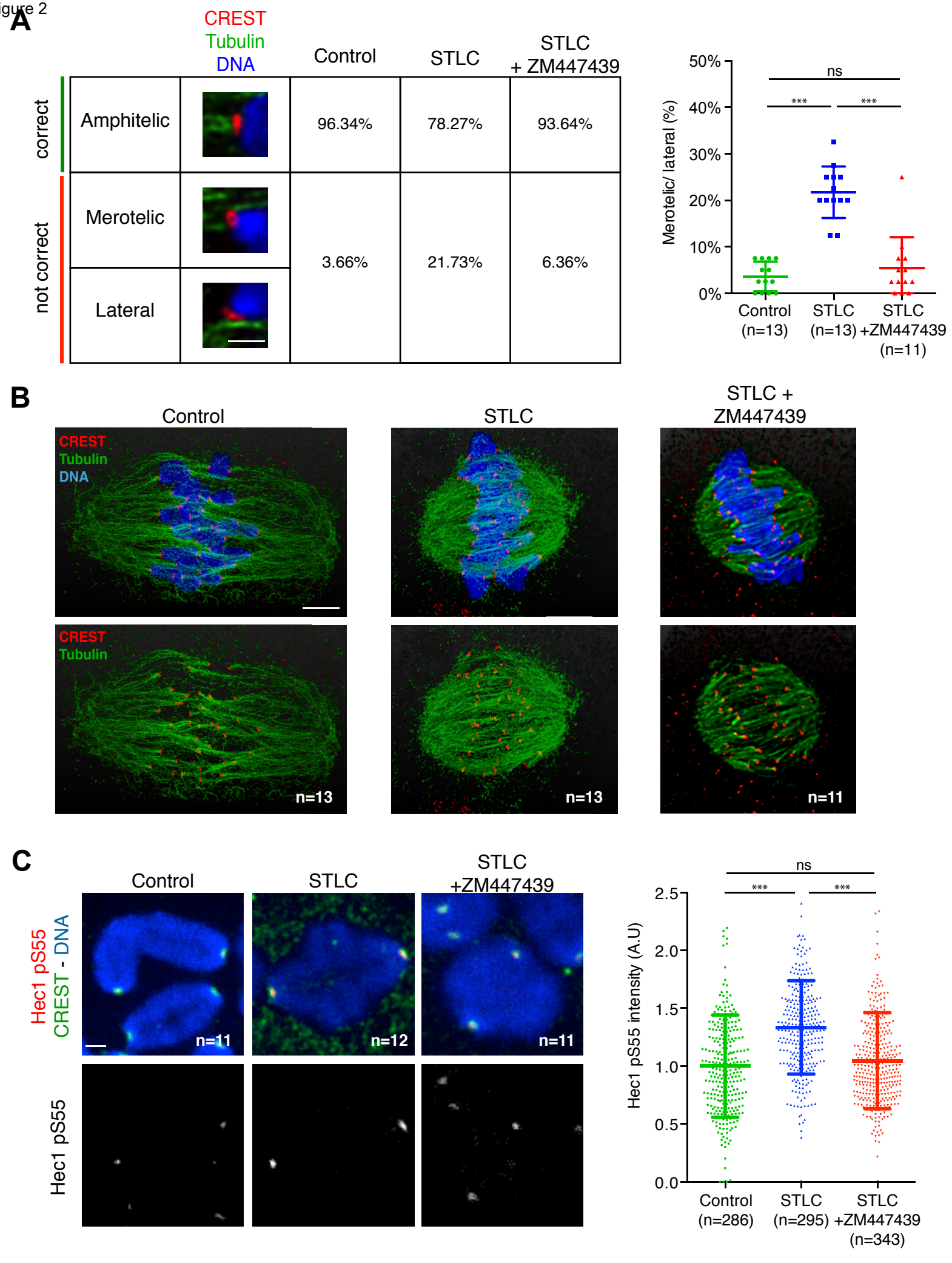
A
CREST
Tubulin
DNA
Control
STLC
STLC + ZM447439
correct
not correct
Amphitelic
Merotelic
Lateral
96.34%
78.27%
93.64%
3.66%
21.73%
6.36%
Merotelic/ lateral (%)
50%
40%
30%
20%
10%
0%
ns
***
***
Control (n=13)
STLC (n=13)
STLC +ZM447439 (n=11)
B
Control
STLC
STLC + ZM447439
CREST
Tubulin
DNA
n=13
n=13
n=11
C
Control
STLC
STLC +ZM447439
Hec1 pS55
CREST - DNA
Hec1 pS55
n=11
n=12
n=11
Hec1 pS55 intensity (A.U)
2.5
2.0
1.5
1.0
0.5
0.0
ns
***
***
Control (n=286)
STLC (n=295)
STLC +ZM447439 (n=343)

Figure 3

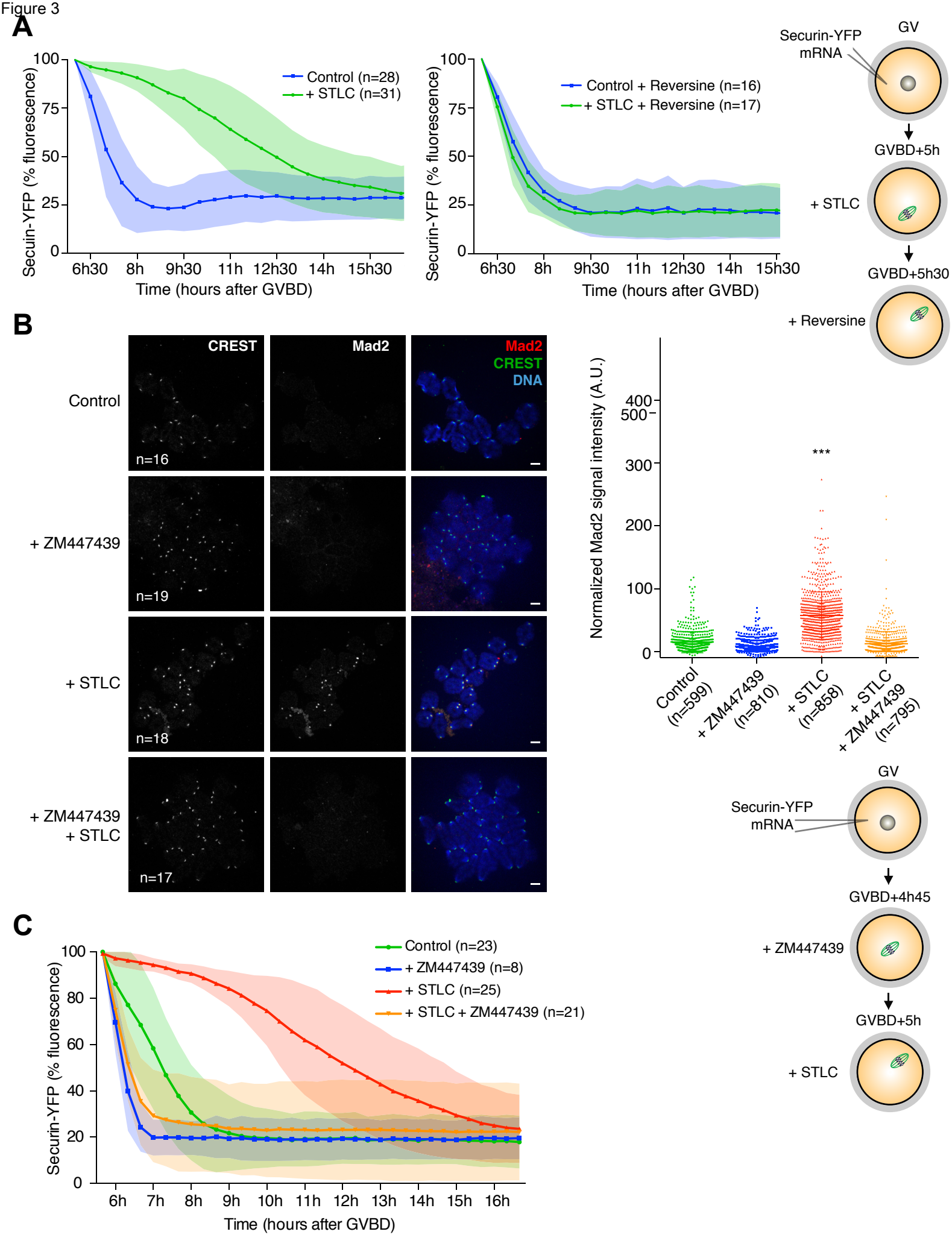
A
Securin-YFP (% fluorescence)
Time (hours after GVBD)
Control (n=28)
+ STLC (n=31)
Control + Reversine (n=16)
+ STLC + Reversine (n=17)
6h30
8h
9h30
11h
12h30
14h
15h30
GV
Securin-YFP mRNA
GVBD+5h
+ STLC
GVBD+5h30
+ Reversine
B
CREST
Mad2
Mad2 CREST DNA
Control
+ ZM447439
+ STLC
+ ZM447439 + STLC
n=16
n=19
n=18
n=17
Normalized Mad2 signal intensity (A.U.)
***
Control (n=599)
+ ZM447439 (n=810)
+ STLC (n=858)
+ STLC + ZM447439 (n=795)
GV
Securin-YFP mRNA
GVBD+4h45
+ ZM447439
GVBD+5h
+ STLC
C
Securin-YFP (% fluorescence)
Time (hours after GVBD)
Control (n=23)
+ ZM447439 (n=8)
+ STLC (n=25)
+ STLC + ZM447439 (n=21)
6h
7h
8h
9h
10h
11h
12h
13h
14h
15h
16h

Figure 4

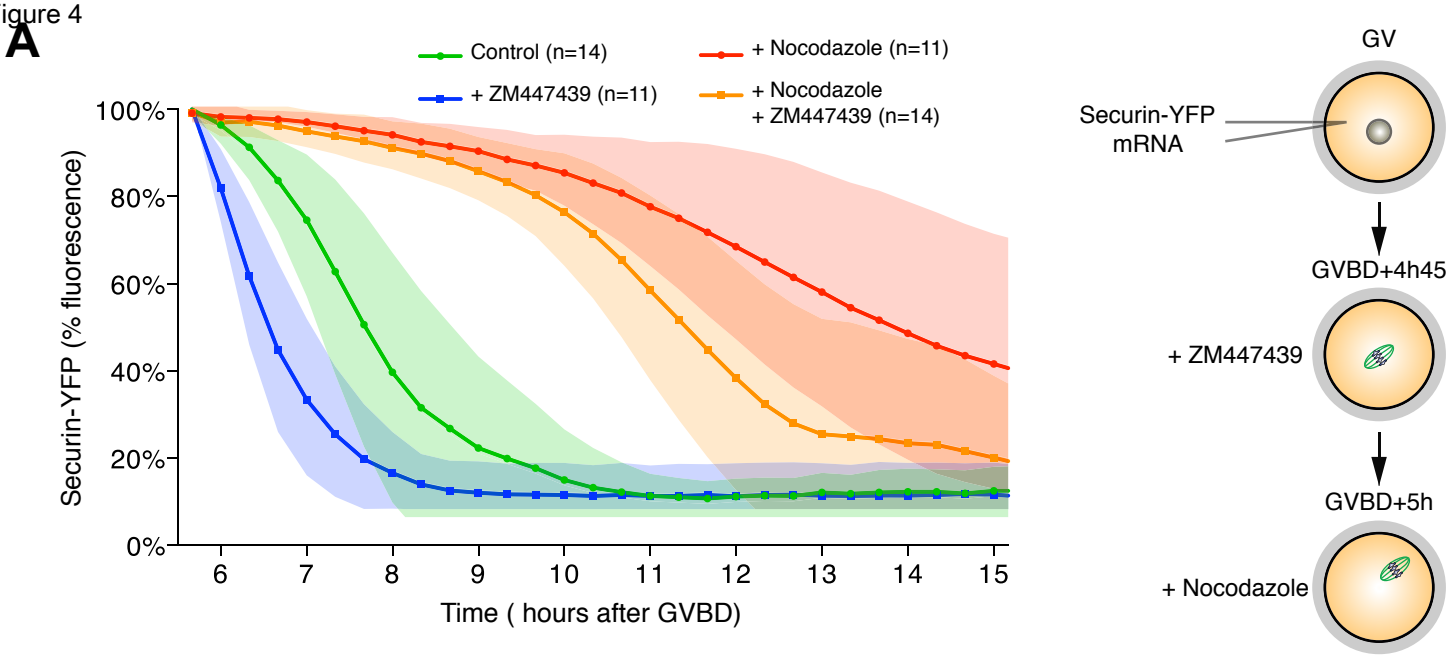
A
Control (n=14)
+ ZM447439 (n=11)
+ Nocodazole (n=11)
+ Nocodazole
+ ZM447439 (n=14)
Securin-YFP (% fluorescence)
100%
80%
60%
40%
20%
0%
6
7
8
9
10
11
12
13
14
15
Time (hours after GVBD)
GV
Securin-YFP
mRNA
GVBD+4h45
+ ZM447439
GVBD+5h
+ Nocodazole

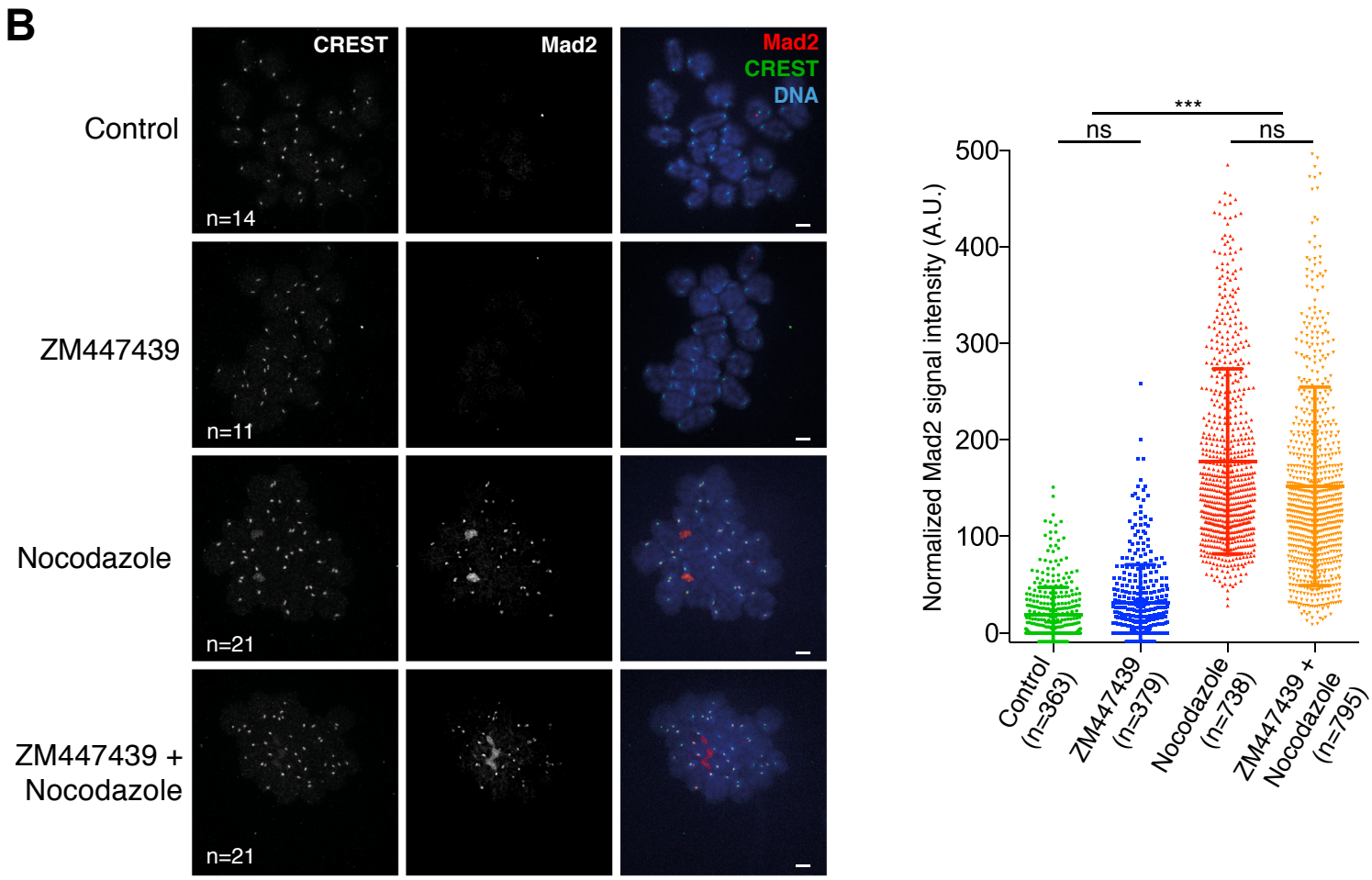
B
CREST
Mad2
Mad2
CREST
DNA
Control
n=14
ZM447439
n=11
Nocodazole
n=21
ZM447439 +
Nocodazole
n=21
***
ns
ns
Normalized Mad2 signal intensity (A.U.)
500
400
300
200
100
0
Control
(n=363)
ZM447439
(n=379)
Nocodazole
(n=738)
ZM447439 +
Nocodazole
(n=795)

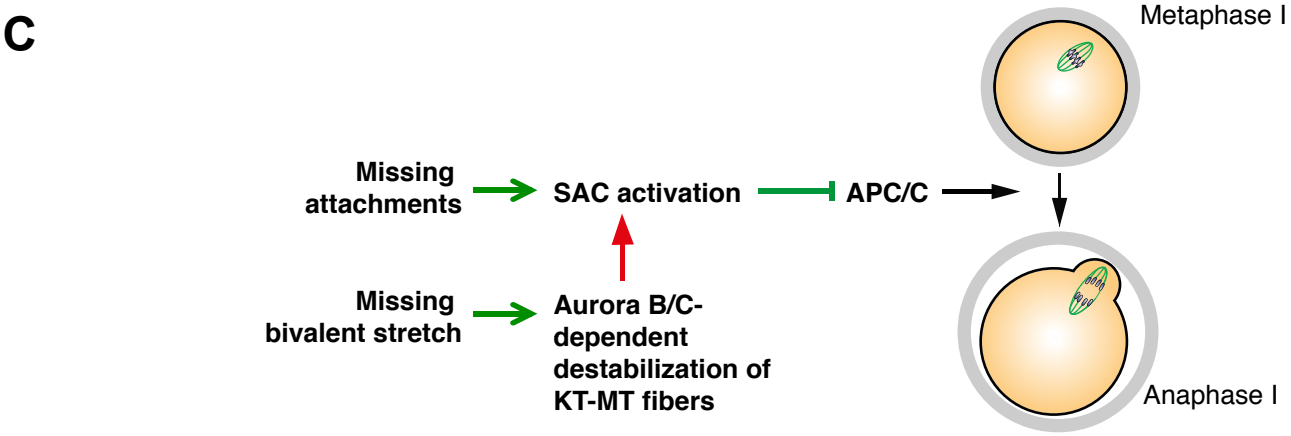
C
Metaphase I
Missing
attachments
SAC activation
APC/C
Missing
bivalent stretch
Aurora B/C-
dependent
destabilization of
KT-MT fibers
Anaphase I

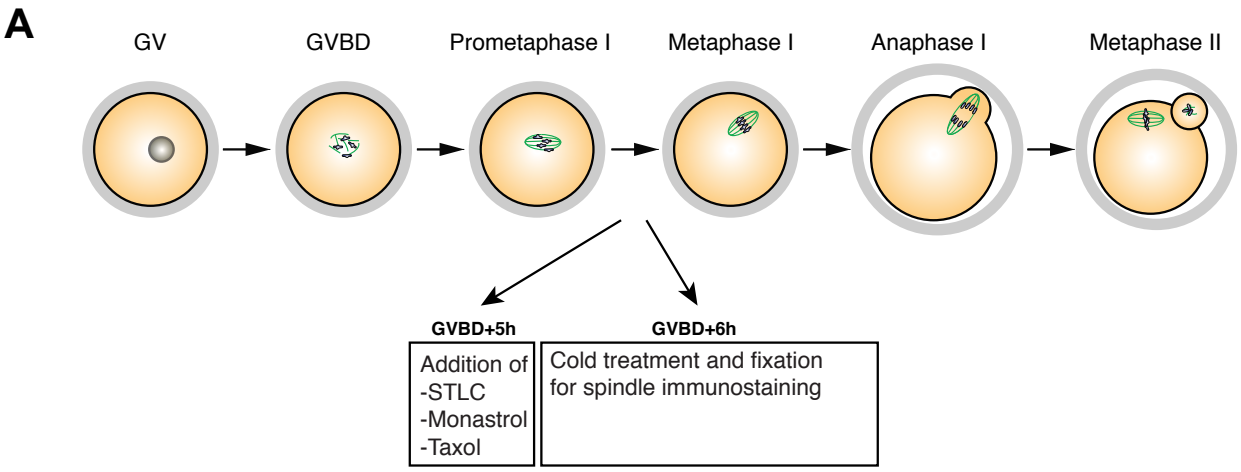
A
GV
GVBD
Prometaphase I
Metaphase I
Anaphase I
Metaphase II
GVBD+5h
GVBD+6h
Addition of
-STLC
-Monastrol
-Taxol
Cold treatment and fixation
for spindle immunostaining

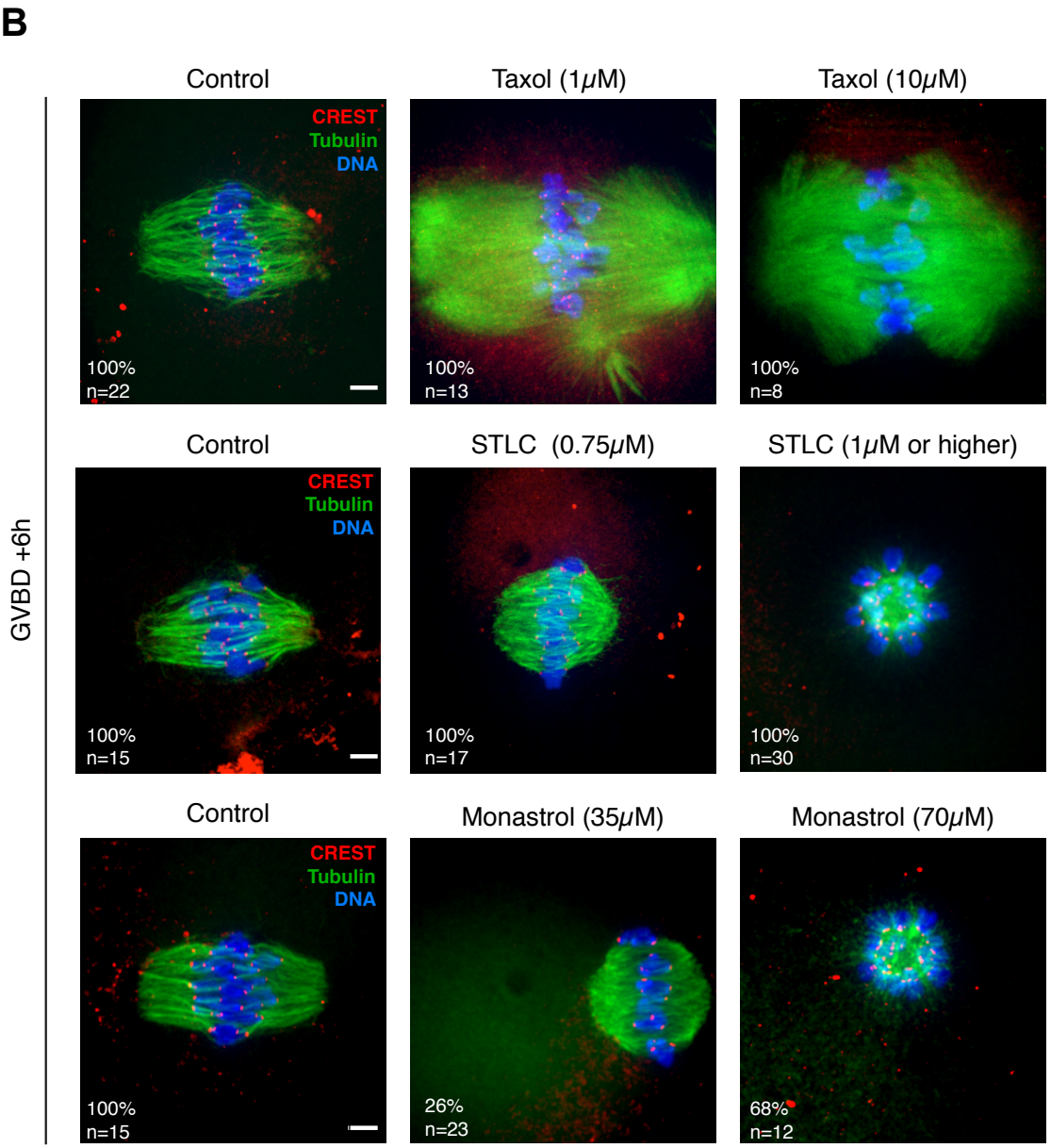
B
GVBD +6h
Control
Taxol (1μM)
Taxol (10μM)
CREST
Tubulin
DNA
100%
n=22
100%
n=13
100%
n=8
Control
STLC (0.75μM)
STLC (1μM or higher)
CREST
Tubulin
DNA
100%
n=15
100%
n=17
100%
n=30
Control
Monastrol (35μM)
Monastrol (70μM)
CREST
Tubulin
DNA
100%
n=15
26%
n=23
68%
n=12

Figure S1. Reducing spindle tension in oocyte meiosis I. Related to Figure 1.
(A) Scheme of the meiotic maturation in mouse oocytes, with experimental set-up indicating when the drugs were added. In mammals, hormonal stimulation induces a small number of oocytes arrested in GV (Germinal Vesicle) stage to enter meiosis I and to progress until metaphase of meiosis II, to await fertilization. Mouse oocytes can be induced *in vitro* to enter the first meiotic division in a synchronized manner, which is visible as Germinal Vesicle Breakdown (GVBD). Taking advantage of the high temporal resolution of prometaphase I in mouse oocytes, we allowed oocytes to form stable bipolar spindles before adding drugs perturbing spindle dynamics. As pools of oocytes can be induced to enter meiosis at approximately the same time (+/- 10 minutes), we were able to study error correction in response to the addition of different drugs affecting bivalent stretch in synchronized populations of oocytes at a time when kinetochores are already attached. Note that STLC, Monastrol or Taxol were always added at 5 hours after GVBD when chromosomes are aligned at the metaphase plate. Subsequent cold treatment and spindle fixation was performed at 6 hours after GVBD. **(B)** Whole-mount immunofluorescence staining of cold-treated spindles from oocytes fixed 6 hours after GVBD. Oocytes were treated with STLC, Monastrol, or Taxol 5 hours after GVBD at the concentrations indicated. Microtubule fibers were stained with anti-Tubulin antibody (green), kinetochores with CREST (red) and chromosomes with Hoechst (blue). Overlays of z-sections covering the whole volume of the spindle (15 to 25µm) are shown. Pictures are representative of the spindle phenotype observed for each condition from at least 2 independent experiments, involving each a total of at least 2 mice (n: number of oocytes). Scale bar: 5µm.

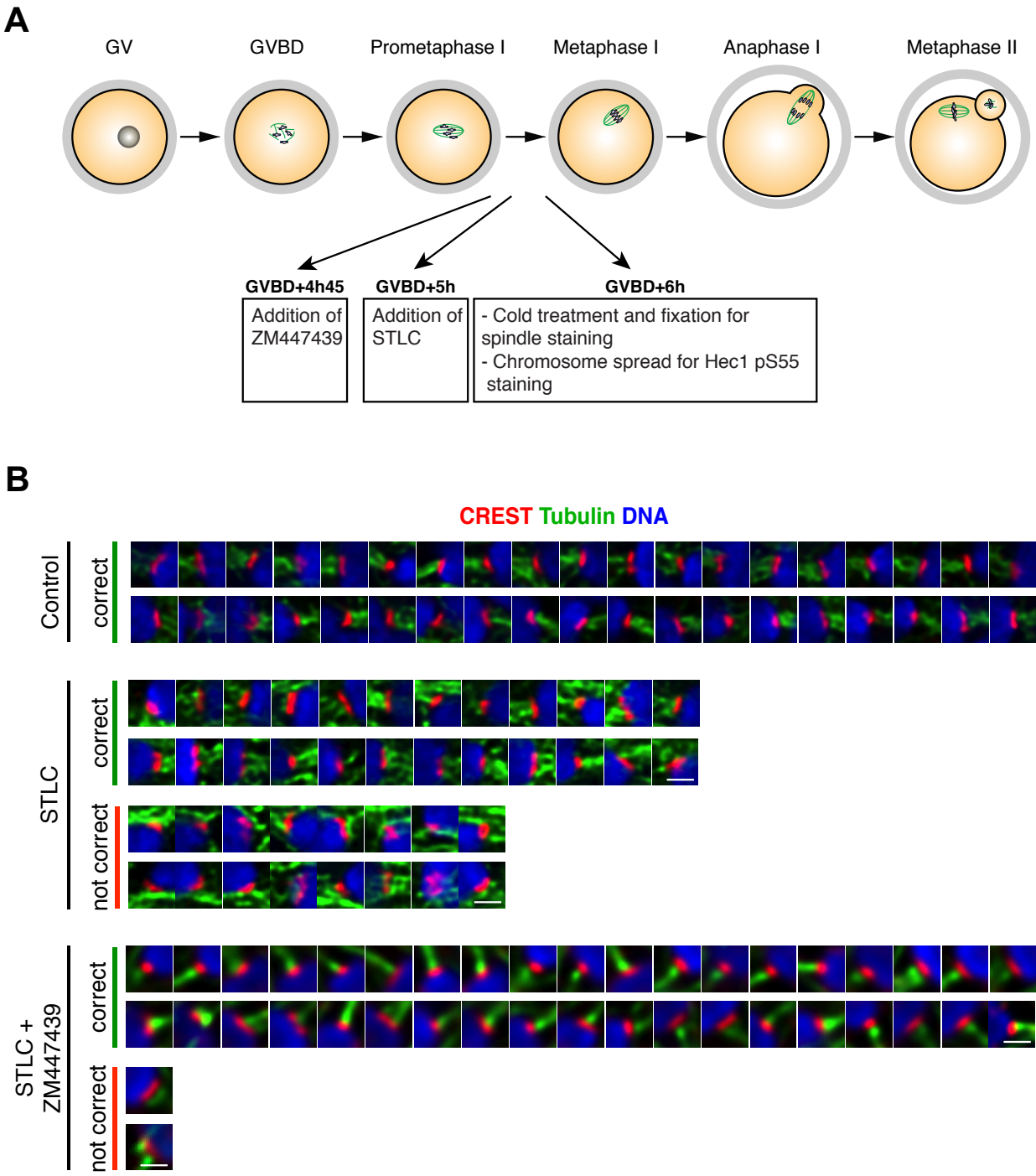

Figure S2. Incorrect microtubule interactions in STLC-treated oocytes depend on Aurora B/C kinase activity. Related to Figure 2.

(A) Scheme of the experimental set-up indicating when the drugs were added and when the subsequent procedures were performed. **(B)** Whole-mount immunofluorescence staining of cold-treated spindles from oocytes fixed 6 hours after GVBD. Spindles were imaged with a confocal microscope, using a workflow enabling near super-resolution pictures. Microtubule fibers were stained with anti-Tubulin antibody (green), kinetochores with CREST (red) and chromosomes with Hoechst (blue). Where indicated, oocytes were treated either with STLC (0.75µM) at 5 hours after GVBD, or additionally with ZM447439 (10µM) 15 minutes prior to STLC treatment. For each condition, correct attachments are shown above, and incorrect (merotelic/lateral) attachments/interactions below. Shown are all 40 kinetochore-microtubule interactions from one representative oocyte for each condition. Scale bar: 2µm.

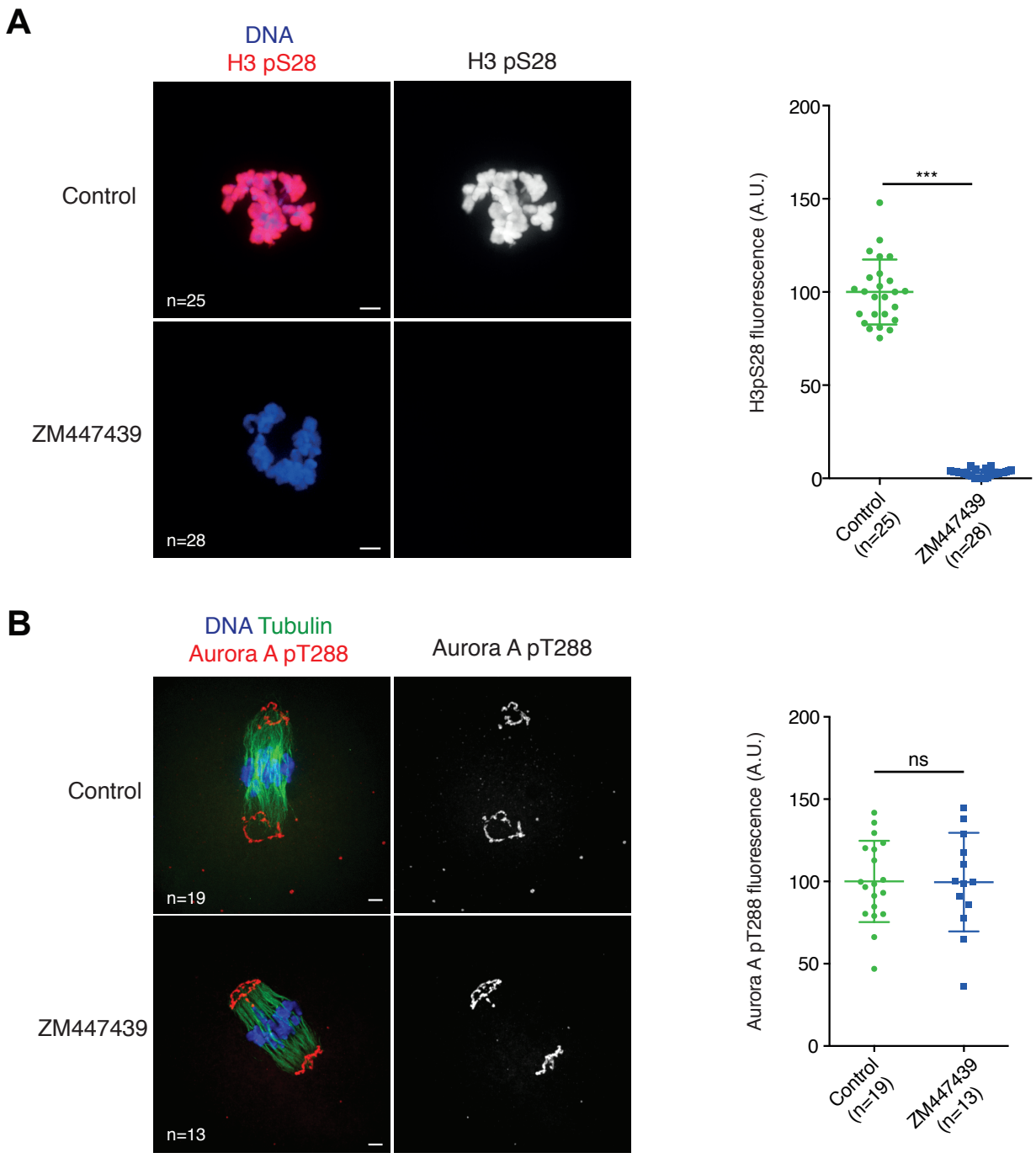

Figure S3. ZM447439 inhibits Aurora B but not Aurora A activity. Related to Figure 2.
(A) Whole-mount immunofluorescence staining of oocytes fixed at 1 hour after GVBD. Where indicated, oocytes were treated with ZM447439 (10µM) at GVBD precisely. (H3S28 becomes phosphorylated at GVBD.) Oocytes were stained with anti-H3 pS28 (red) and Hoechst (blue). The graph on the right shows the distribution of H3 pS28 signal intensities measured for each oocyte, and normalized to the control mean for each experiment. n: number of oocytes, two independent experiments involving a total of at least of 2 mice have been performed. **(B)** Whole-mount immunofluorescence staining of cold-treated spindles of oocytes fixed 6 hours after GVBD. Where indicated, oocytes were treated with the drug ZM447439 (10µM) at 4 hours 45 minutes after GVBD. Oocytes were stained with anti-Tubulin antibody (green), anti-Aurora A pT288 antibody (red) and Hoechst (blue). The graph on the right shows the distribution of Aurora A pT288 signal intensities measured for each oocyte, and normalized to the control mean for each experiment. n: number of oocytes. Two independent experiments involving a total of at least 2 mice have been performed. For (A) and (B) p values were calculated with two-tailed unpaired Student's t-test (not significant [ns] p value > 0.05, *** p value <0.0001). Error bars show Standard Deviation. Scale bar: 5µm.

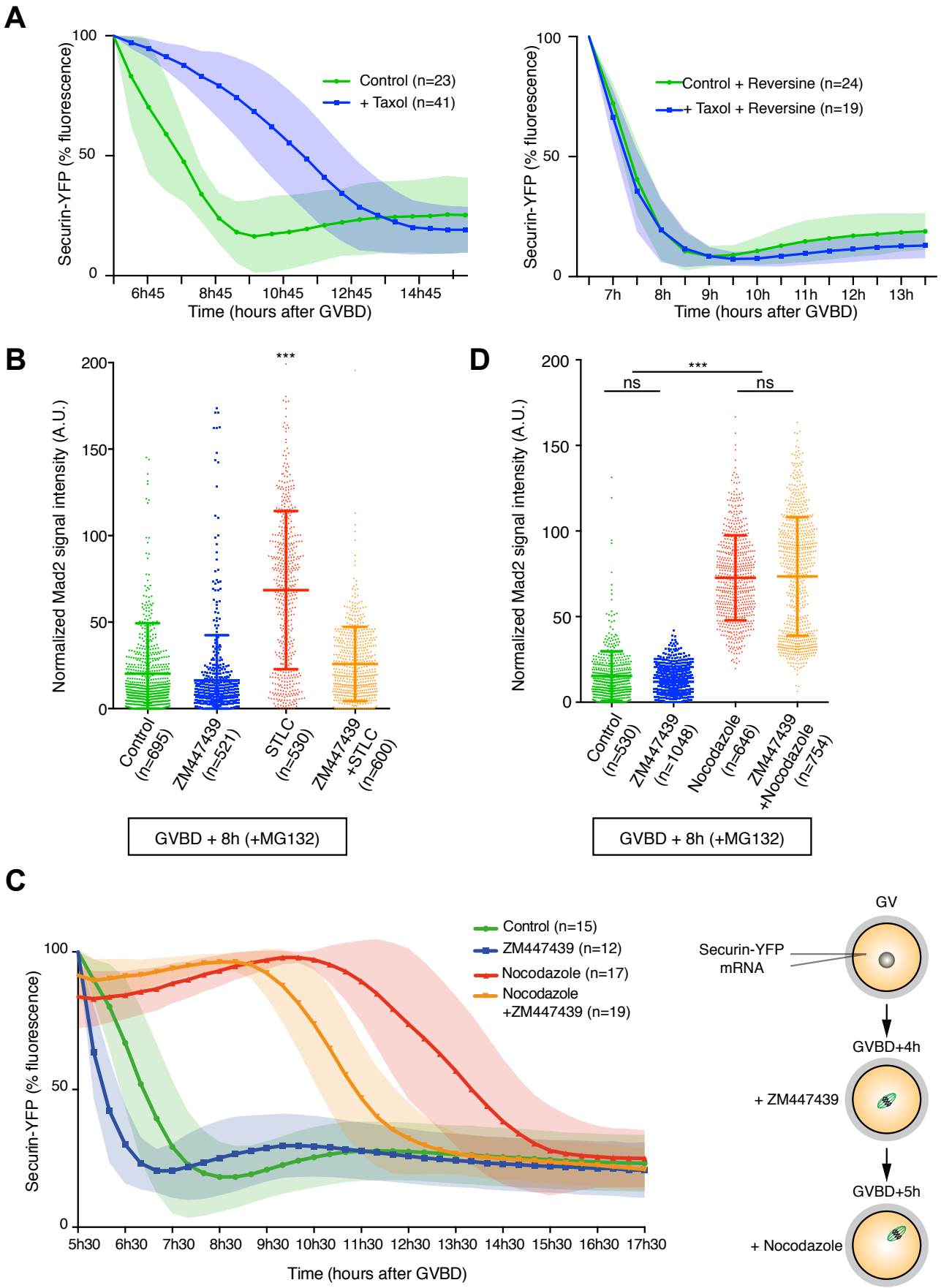
A
Securin-YFP (% fluorescence)
100
50
0
Control (n=23)
+ Taxol (n=41)
6h45
8h45
10h45
12h45
14h45
Time (hours after GVBD)
Control + Reversine (n=24)
+ Taxol + Reversine (n=19)
7h
8h
9h
10h
11h
12h
13h
B
Normalized Mad2 signal intensity (A.U.)
200
150
100
50
0
***
Control (n=695)
ZM447439 (n=521)
STLC (n=530)
ZM447439 +STLC (n=600)
GVBD + 8h (+MG132)
D
ns
ns
Control (n=530)
ZM447439 (n=1048)
Nocodazole (n=646)
ZM447439 +Nocodazole (n=754)
C
Control (n=15)
ZM447439 (n=12)
Nocodazole (n=17)
Nocodazole +ZM447439 (n=19)
5h30
6h30
7h30
8h30
9h30
10h30
11h30
12h30
13h30
14h30
15h30
16h30
17h30
GV
Securin-YFP mRNA
GVBD+4h
+ ZM447439
GVBD+5h
+ Nocodazole

Figure S4. Securin degradation and Mad2 levels in either taxol or nocodazole-treated oocytes. Related to Figure 3 and 4.

(A) Oocytes were injected with Securin-YFP encoding mRNA at GV stage. Where indicated, oocytes were treated with Taxol (1µM) at 5 hours after GVBD and with Reversine (0.5µM) at 5.5 hours after GVBD. Securin-YFP signal intensity was monitored by time-lapse fluorescence imaging and normalized to the highest value for each oocyte. Mean and standard deviation of the population are plotted in arbitrary units against time. Two independent experiments involving a total of at least 4 mice have been performed. n: number of oocytes. **(B)** Graph showing the distribution of Mad2 signal intensities normalized to CREST measured on chromosome spread stained as in Figure 3B and Figure 4B. Oocytes were treated with MG132 (20µM) at 4 hours 45 minutes after GVBD and spread 8 hours after GVBD. Oocytes were treated with the drug ZM447439 (10µM) at 4 hours 45 minutes after GVBD, prior to STLC (0.75µM) treatment at 5 hours after GVBD. The values corresponding to all kinetochores measured are displayed (n: number of kinetochores). Statistical analysis was performed on the mean value calculated for each oocyte (n= 27 for control, n= 18 for ZM447439, n= 22 for STLC, and n= 21 for ZM447439+STLC). See (D) for statistics. **(C)** As indicated on the scheme on the right, oocytes were injected with Securin-YFP encoding mRNA at GV stage, and treated with the drug ZM447439 (10µM) at 4 hours after GVBD, prior to Nocodazole treatment (400nM) at 5 hours after GVBD. YFP signal intensity was monitored by time-lapse fluorescence imaging and normalized to the highest value for each oocyte. Mean and standard deviation of the population are plotted in arbitrary units against time. Two independent experiments involving a minimum of 4 mice have been performed. n: number of oocytes. **(D)** Graph showing the distribution of Mad2 signal intensities normalized to CREST measured on chromosome spread stained as in (B). Oocytes were treated with MG132 (20µM) at 4 hours 45 minutes after GVBD and spread 8 hours after GVBD. Oocytes were treated with the drug ZM447439 (10µM) at 4 hours 45 minutes after GVBD, prior to Nocodazole (400 nM) treatment at 5 hours after GVBD. The values corresponding to all kinetochores measured are displayed (n: number of kinetochores). Statistical analysis was performed on the mean value calculated for each oocyte (n= 22 for control, n= 32 for ZM447439, n= 23 for Nocodazole, and n= 26 for ZM447439+Nocodazole). For (B) and (D) three independent experiments involving a total of at least 6 mice have been performed. p values were calculated with two-tailed unpaired Student's t-test (not significant [ns] p value > 0.05, ***p value < 0.0001). Error bars show Standard Deviation.